

# Characterization and Applicability of Low-Background Germanium Detectors

by Ronald M. Keyser

*EG&G ORTEC, Inc, 100 Midland Road, Oak Ridge, TN 37831-0895 U.S.A.*

## Introduction

The radiation background of standard cryostats is sufficiently low for the majority of germanium detector applications. There are, however, some measurement situations that require low radiation background detector cryostats. The use of low-background cryostats lowers the Minimum Detectable Activity (MDA). This is very important, for example, when measuring environmental samples and foodstuffs.

The term "low background" currently is not well defined. In this review, a method of specifying or quantifying the background qualities of a detector is proposed, so as to establish a common terminology for the use of manufacturers and users.

Low-background HPGe detectors are usually considered to be detector assemblies or systems that contribute little or nothing compared to the sample spectrum being collected by the detector. If samples being analyzed possess very little activity, the contribution from the materials near the detector must be minimized, to reduce the counts in the detector from materials other than the sample being analyzed. This improves the signal-to-noise ratio, which reduces the uncertainty of the calculated activity and the MDA.

The activity of a low background or even normal background detector cryostat can only be quantified in a reasonably well-constructed shield. Shields typically are made of selected lead with a lining of lower atomic number (Z) material to absorb secondary lead X-rays. Figure 1 shows the spectrum from a low-background detector measured in a copper-lined lead shield, which reduces the external background to a low level. Compare this with Fig. 2, which shows an unshielded detector. The major peaks are at 511, 1460, and 609 keV. To gain a perspective on the low levels of activity required for a detector to be called "low-background," Fig. 3 shows a spectrum of drinking water taken with the same detector, shield, and live time as Fig. 1.

## Detector Construction

To understand how various components contribute to the background of the detector, it is helpful to examine a typical germanium detector's construction. Figure 4 shows a cutaway view of a typical low-background detector. It is important to consider which materials in the detector cryostat are closest to the detector element and which are the most massive. The detector element itself is nearly uniformly sensitive to gamma rays from all directions.

The cryostat materials closest to the detector are the mounting cup, endcap, entrance window, and the mounting pedestal. The pedestal and mounting cup are OFHC copper. The endcap is selected magnesium. The entrance window is selected magnesium or selected beryllium. Other materials (for example, the electronics package, the thermal insulator, and the cooling rod) are partially shielded from the detector element by the pedestal and a lead back-shield (if installed).

Aluminum usually contains primordial contamination, and Fig. 5 shows a typical spectrum for a 2-kg sample of aluminum. Table 1 lists the peaks visible in the spectrum. For comparison, Fig. 6 shows a spectrum from the same detector/shield with a blank sample. Figure 7 shows the spectrum for normal beryllium compared to selected low-background beryllium. Table 2 lists the peaks visible in the beryllium spectrum.

In order to produce the best low-background detectors, it is clear that every large mass component close to the detector must be selected to be as low-level as possible. Every raw material component must be measured for activity before being used. In some cases conventional materials, such as aluminum, cannot be found with sufficiently low background and thus are replaced by a similar material (for example, magnesium).

After assembly from selected materials, the detector background is measured in a shield. Figure 8 shows a typical, low-cost shield facility. Figure 9 shows a typical spectrum, and Table 3 lists the peaks in the spectrum.

### How Low Background is Quantified

The problem now is to quantify the low-background features of spectra in a useful and meaningful way; that is, in a way that will allow the user to relate the reported numbers to the MDA values that can be expected when using the detector. While the actual MDAs obtainable cannot be easily quantified, one can certainly ascertain whether one detector will have lower background and MDAs than another detector when both are used in a specific laboratory shield.

There are three common, but not equally valid, methods of specifying the user's requirements: (1) that there be no more than a specified activity of each of a list of nuclides present in the detector, (2) that the average number of counts per second per unit energy, at selected energies, be below a particular level, and (3) that there be no peaks in the spectrum at selected energies. The energies selected can be the whole useful energy range, meaning that these numbers would represent the background over the entire range of the detector.

The first method, nuclide activity, is not appropriate for specifying the background because the conversion factor from the net counts in the spectrum to activity depends on the source-detector geometry of the calibration source. This efficiency factor (in becquerels/counts/sec) is only strictly valid for the geometry of the calibration source. The

efficiency factor is needed to calculate the MDA (which is in units of activity) for a given background level. While the peak countrate for the background can be converted to activities for this geometry, a different geometry or efficiency factor will yield a different activity for the same background spectrum.\* Table 4 shows the activity calculated for a single spectrum based on two efficiency calibrations: a 1-liter Marinelli beaker and a point source 10 cm from the endcap.

Thus, while the user is necessarily concerned with activity, specifying the background activity is not a good way of specifying low-background performance.

The second method, specification of the average background counts, is useful if correctly calculated and applied. The spectrum consists of full-energy counts and non-specific or continuum counts. The non-specific counts can be partial capture of full-energy gamma-rays or full capture of photons that have been degraded outside the detector. If this histogram of counts is expressed as counts/sec/keV, at energy E, then it can be used to estimate the background of the detector. The user can then convert this to MDA, using his preferred MDA formula.

The spectrum channel data should be averaged over a number of channels equivalent to about 5 times the resolution of the detector at the energy specified. Much larger widths can obscure real structure (such as Compton edges) in the spectrum, and smaller widths do not sufficiently remove the statistical variation in the channel counts. The smoothing or averaging width should always be chosen as a multiple of the FWHM of the detector, because it is this width or number of channels that will be the background under the peak at that energy. The choice of 5 times the FWHM assures the inclusion of any neighboring structure in the spectrum that will affect the background. The formula for this is:

$$B(E) = \frac{G}{5n(E) + 1} \sum_{i=j-2.5n(E)}^{j+2.5n(E)} C_{j+i}$$

where  $j$  = channel corresponding to energy  $E$   
 $B(E)$  = smoothed background at energy  $E$   
 $G$  = conversion factor from channels to energy  
 $C_i$  = channel contents of channel  $i$   
 $n(E)$  = detector resolution at energy  $E$

Figure 10 shows part of a spectrum for a 72% efficiency detector with a resolution of 1.84 keV at 1.33 MeV. This spectrum was collected for 100,000 seconds. The energy region is centered at 661 keV. Note the fluctuations in the data and the calculated background.

---

\*The values used for the gammas/disintegration and half-life of the isotope will also affect the efficiency factor.

This number,  $B(E)$ , for the average background describes the overall spectrum and is useful for predicting results where there are no peaks in the background. However, there are certain nuclides of interest that also appear naturally or have lines that are close to lines from naturally occurring nuclides. In these cases it is also important that these naturally occurring nuclides be minimized.

Figure 11 shows the spectrum from unselected aluminum in the region of 92 keV. This peak is from  $^{234}\text{Th}$ . The average background is also shown. If any peak of interest is near 92 keV, then the MDA for this isotope will be affected by the extent of this background peak. If the peak of interest is this peak (or one within a few keV), then special subtraction techniques must be used to correct for this background peak. This affects the uncertainty of the result and the MDA, because one may well be subtracting nearly equal numbers.

The third method, specifying maximum acceptable peak areas at selected energies, is useful to identify problem areas, but again must be calculated correctly. When the peak is visible, as in Fig. 11, there is little question about the area of the peak. However, if there is a very small peak or no peak, there is doubt about the area of the peak. There is also the question of the maximum peak area that could be hidden in the background spectrum. Figure 12 shows the same peak as Fig. 11, but with three different regions of integration for determining the background and net peak area. Note that even in this case of a well-defined peak, the areas differ by more than 10%. Figure 13 shows the energy region near 46 keV for the same spectrum. Also shown is a region corresponding to 2 times the FWHM of the detector. As this region is moved across the spectrum one channel at a time and the new peak area generated, the peak area will change as the ends of the region pass over the ups and downs of the channel contents. This variation is shown in table 5. The variation in the area of a very small peak can be more than a factor of 10 as the end points of integration are varied over a short range of channels. This poses the problem of what net area to report for these small peaks. Several authors<sup>1,2,3</sup> report on what peak area can be considered to be a real peak with a given error and confidence level; but, without a strict definition of how to calculate the peak area in a given region, no valid test can be made.

Two peak area calculation methods have been defined<sup>4,5</sup> and can be used to define the peak area of small peaks. One method assumes the peak exists. The background is defined on both sides of the peak as the average counts in a region that is 1.5 times the FWHM of the detector. The gross peak area is the sum of the channels corresponding to 3 · FWHM. The net peak area is the gross minus the average background for 3 times the FWHM. This is shown in Fig. 14.

Another method is to determine the maximum peak hidden in the background. This is calculated as the square root of the average background per channel times the number of channels in the FWHM. The average background per channel is the sum of the channels in a region 2.5 times the FWHM, divided by the number of channels in the sum. Here the peak region is integrated, meaning that this overestimates the peak, if the "hidden" peak exists. Table 6 shows a comparison of these two methods for several cases (small visible peak, high background, low background). For low-background specifications, both methods

can be used. Other methods could also be used, so long as they are described and produce consistent results.

Thus, there are two sets of values to be specified for characterization of a low background number:

1. The average counts/sec/keV, averaged over  $5 \times \text{FWHM}$
2. the peak area and uncertainty at selected energies (by either of two methods)

Figure 16 shows the average counts/sec/keV for a specific detector compared to the peak area, calculated as in Fig. 15.

Obviously, the larger the continuum background and the more peaks in the background, the higher the MDAs will be. In addition, the resolution and peak-to-Compton ratio (6) affect the MDAs.

## Results

To test the utility of these definitions, a series of low-background detector spectra were collected and the results analyzed using these formulas.

Each low-background detector's background was measured in one of the shields shown in Fig. 8. The energy range measured is about 20 keV to 2.8 MeV for conventional and reverse-electrode coaxial detectors and 10 keV to 800 keV for large-diameter-to-length reverse electrode coaxial detectors. The energy and peak shape calibration was done using an NBS 4275 mixed europium point source standard, 10 cm from endcap. The calibration is done outside the shield. The background spectra were collected for 100,000 seconds inside the shield. An analysis of each spectrum for peak areas at selected energies was done for the peak energies in Table 6.

Figure 17 shows the average background results for a wide range of detectors at selected energies as a function of detector efficiency (and also peak-to-Compton ratio). Figure 18 shows several peak areas as a function of detector efficiency.

These data show that these ways of describing the background and peak areas is an easy-to-use and workable method of specifying the background for HPGe detectors to be used in environmental counting.

## References

1. R. C. Brown and G. L. Troyer, Estimated Minimum Detectable Activity in a Gamma Energy Analysis System, Westinghouse Hanford Co. #WHC-SA-0819-FP, June 1990.
2. L. A. Currie, "Limits for Qualitative Detection and Quantitative Determination, Applications to Radiochemistry," *Analytical Chemistry*, Vol. 40, No. 3, March 1968.
3. J. S. Yadav, J. Brückner, and J. R. Arnold, "Weak Peak Problem in High Resolution Gamma-Ray Spectroscopy," *NIMA*, 277, 1989.
4. *The Analytical Methods of Germanium Radiation Detectors*, Handbook of the Japanese Agency for Science and Technology.
5. Messung und Überwachung der Ableitung gasförmiger und aerosolgebundener radioaktives Stoffe, KTA 1503.1 FASSUNG 2/79.

PEAK CHANNEL	CENTROID ENERGY	BACKGRND COUNTS	NET AREA COUNTS	SUSPECTED NUCLIDE
186.57	62.74	1135.	156.	TH-234
225.58	75.73	2206.	331.	PA-233
274.93	92.17	2536.	1492.	At-xray
429.29	143.58	1559.	552.	U-235
486.13	162.52	1411.	189.	BA-140
554.70	185.35	1779.	1803.	U-235
713.43	238.22	1724.	2059.	PB-212
897.45	299.51	671.	145.	TH-227
1012.98	337.99	497.	143.	AC-228
1052.82	351.26	754.	329.	CE-143
1531.97	510.85	732.	1283.	LA-140
1673.93	558.13	251.	89.	EU-154
1748.29	582.90	361.	771.	TL-208
1826.51	608.95	378.	212.	BI-214
2181.61	727.22	205.	149.	I-132
2298.91	766.29	275.	148.	PA-234M
2518.23	839.34	124.	54.	PB-214
2733.36	910.99	185.	137.	AC-228
3004.07	1001.16	156.	271.	PA-234M
3445.24	1148.10	31.	40.	ZR-97
5918.99	1972.02	21.	27.	-
7152.49	2382.86	23.	36.	-
7776.18	2590.59	4.	12.	-
7855.54	2617.02	31.	309.	TL-208

Table 1

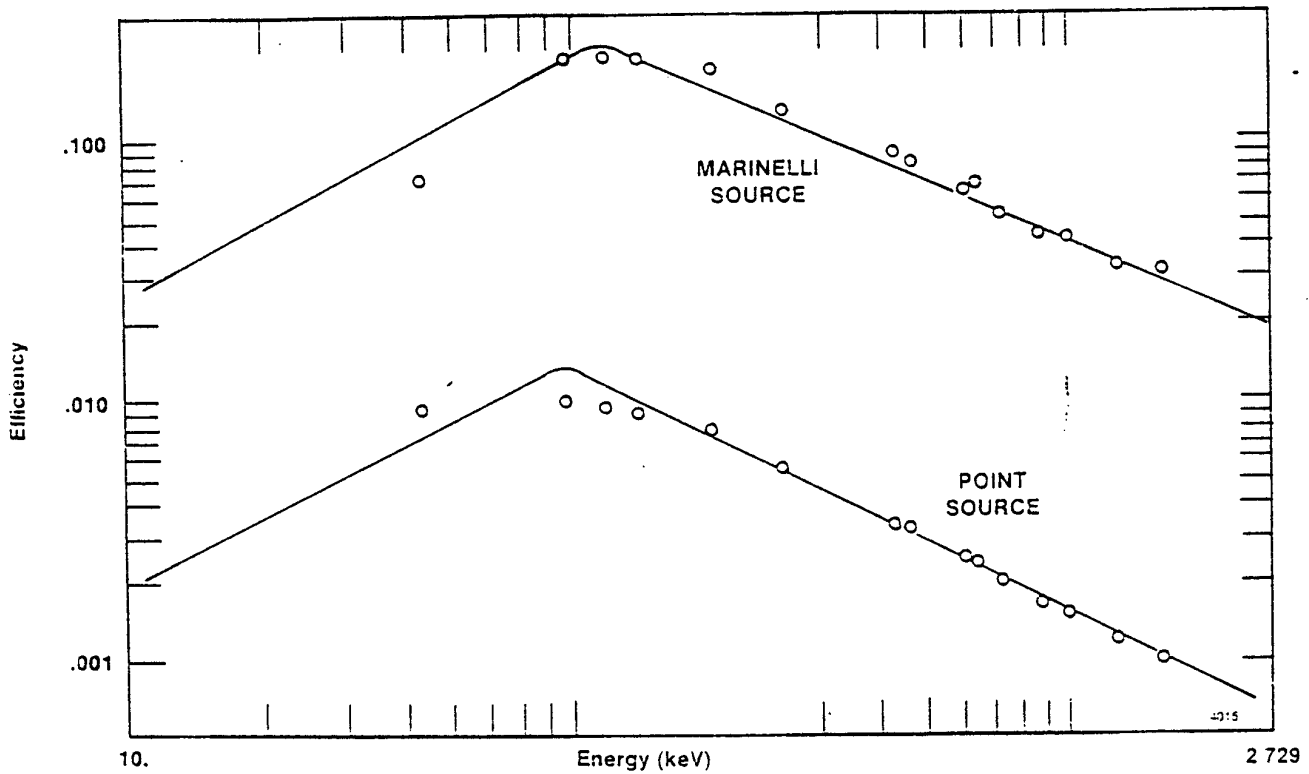
PEAK CHANNEL	CENTROID ENERGY	BACKGRND COUNTS	NET AREA COUNTS	SUSPECTED NUCLIDE
48.14	16.90	26301.	16406.	-
76.16	26.24	3126.	1000.	U-237
146.18	49.56	2126.	222.	NP-239
176.38	59.62	3806.	5844.	U-237
187.83	63.44	2960.	5121.	TH-234
249.90	84.12	2402.	527.	TH-228
275.47	92.64	2556.	8527.	Po-xray
293.24	98.55	1255.	360.	U-xray
335.71	112.70	2275.	357.	TH-234
429.28	143.87	1423.	636.	U-235
488.38	163.56	1324.	355.	PM-151
554.39	185.55	1520.	2811.	U-235
1531.09	510.92	1072.	1376.	LA-140
2198.77	733.35	220.	89.	PA-234
3912.37	1304.20	77.	59.	-
4386.25	1462.06	120.	106.	K-40
6981.07	2326.48	10.	35.	-

Table 2

PEAK CHANNEL	CENTROID ENERGY	BACKGRND COUNTS	NET AREA COUNTS	SUSPECTED NUCLIDE
63.40	23.71	3364.	244.	-
191.62	66.36	1496.	323.	PM
214.02	73.81	3264.	455.	CE
585.86	197.50	5275.	330.	ND
598.45	201.69	4138.	383.	U-
707.82	238.07	4068.	520.	PB
1048.76	351.48	2083.	522.	PB
1526.96	510.55	2657.	2520.	I-
1710.60	571.63	1613.	263.	AS
1744.38	582.87	1622.	391.	TL
1823.00	609.02	1951.	819.	BI
2003.97	669.22	1056.	155.	I-
2132.86	712.09	943.	132.	SB
2505.19	835.94	1038.	205.	AC
2729.93	910.70	854.	451.	I-
2904.83	968.88	964.	171.	AC
2885.63	962.49	1115.	372.	EU
3218.99	1073.38	596.	166.	-
3358.63	1119.83	536.	420.	BI
4223.92	1407.66	499.	157.	BI
4382.30	1460.34	472.	6026.	K-
4527.86	1508.77	342.	183.	BI
4767.24	1588.39	207.	82.	AC
5295.68	1764.17	208.	579.	BI
5543.87	1846.73	163.	182.	Y-
7067.08	2353.41	59.	34.	-
7852.30	2614.60	84.	1355.	TL

Peak	Energy (keV)	Efficiency-Corrected Counts/1000 sec	
		Point	Marinelli
1	241.79	105.3	4.3
2	294.95	271.9	11.0
3	351.70	501.5	20.0
4	609.15	615.4	23.3
5	665.07	27.2	1.0
6	768.28	79.9	3.0
7	934.07	56.1	2.0
8	1120.30	227.5	8.1
9	1155.07	43.9	1.6
10	1238.23	101.0	3.6
11	1280.40	42.4	1.5
12	1377.91	85.0	3.0
13	1631.65	25.1	.9
14	1764.91	249.0	8.5
15	2017.36	19.6	.7
16	2204.24	96.8	3.2
17	2447.85	54.1	1.8

Table 4



Channel		Gross Area	Net Area
Start	Stop		
130	146	1459	-88
129	145	1440	5
128	144	1455	7
127	143	1452	113
126	142	1485	65
125	141	1497	70
124	140	1518	32

Table 5

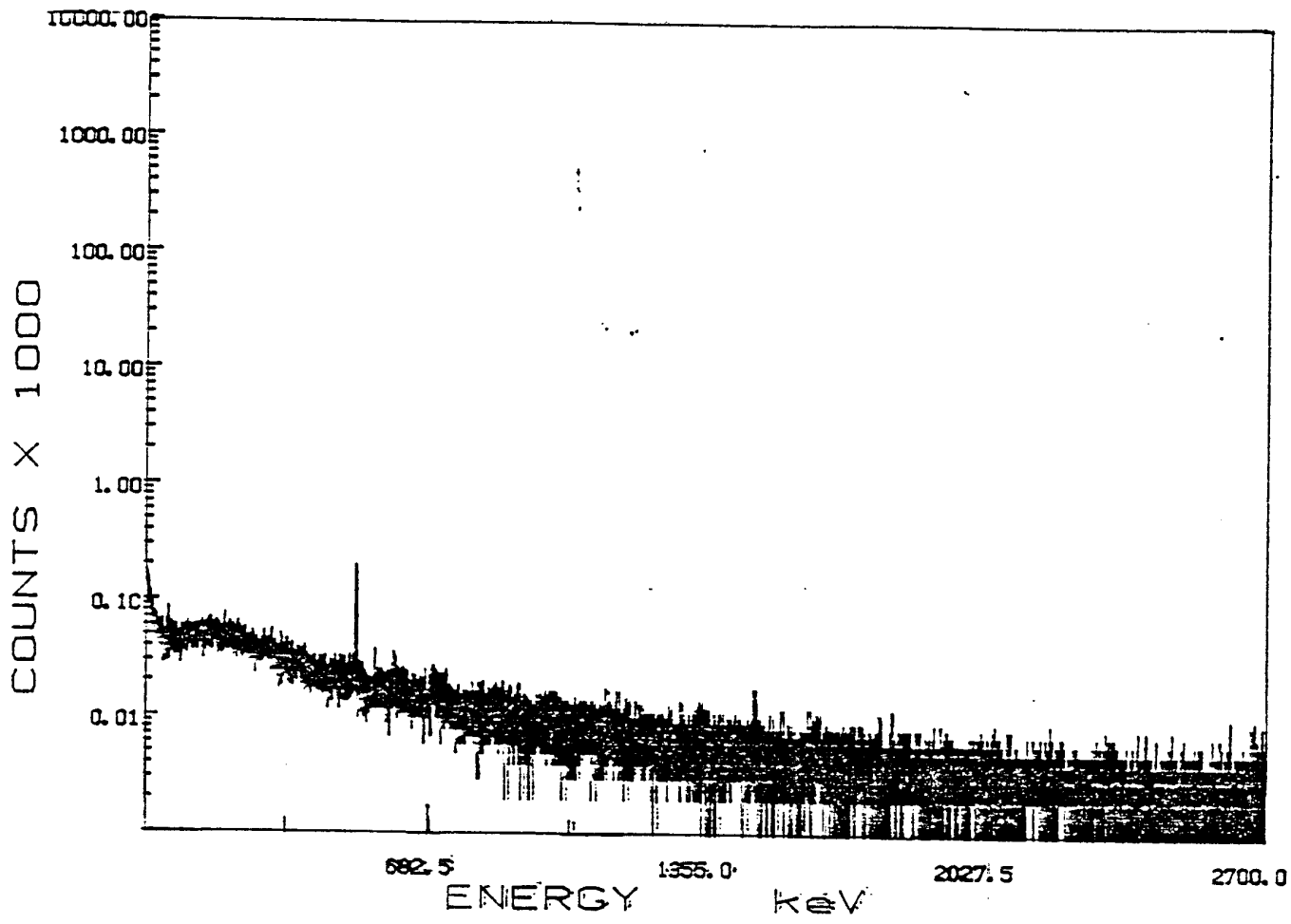


Figure 1

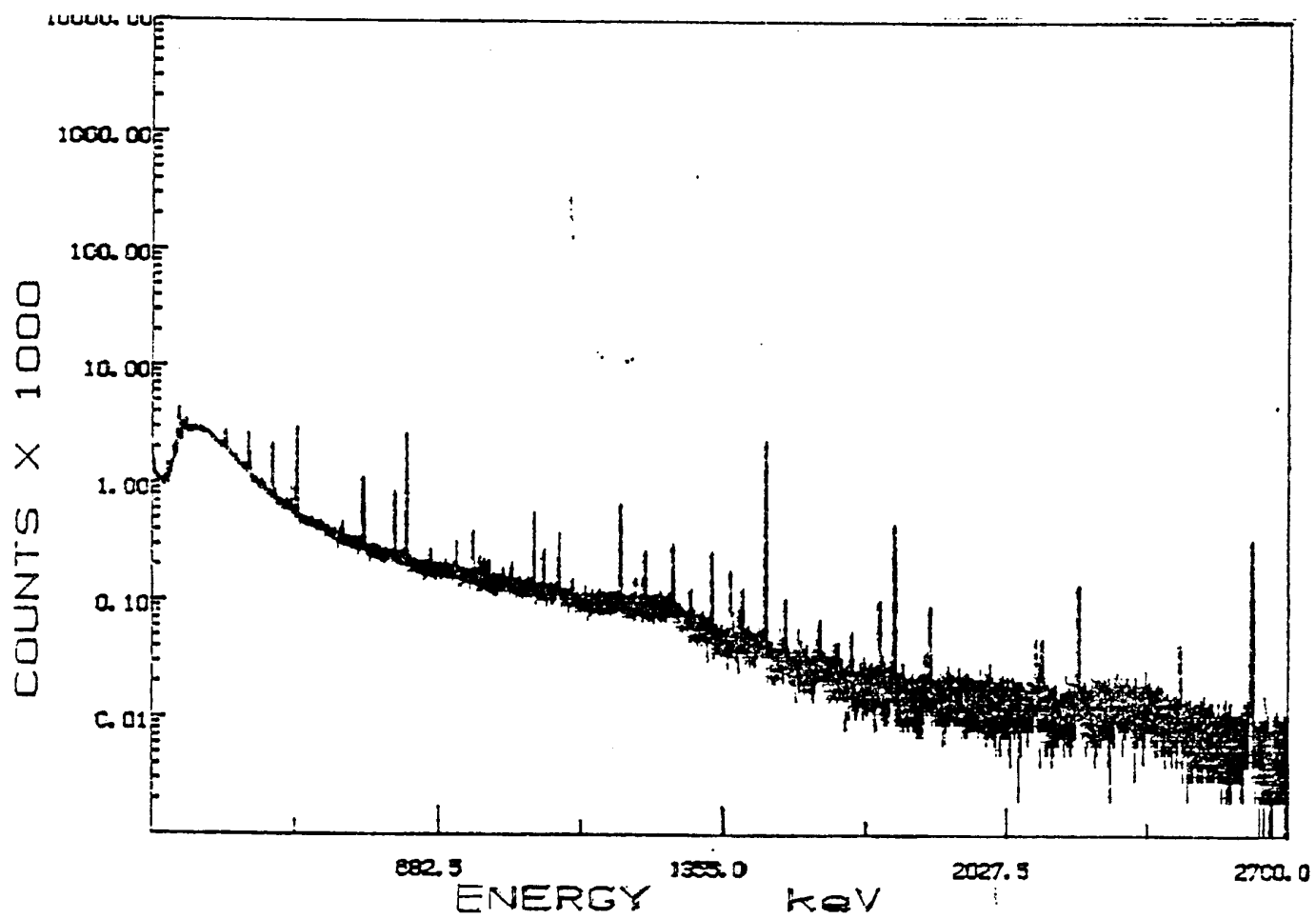


Figure 2

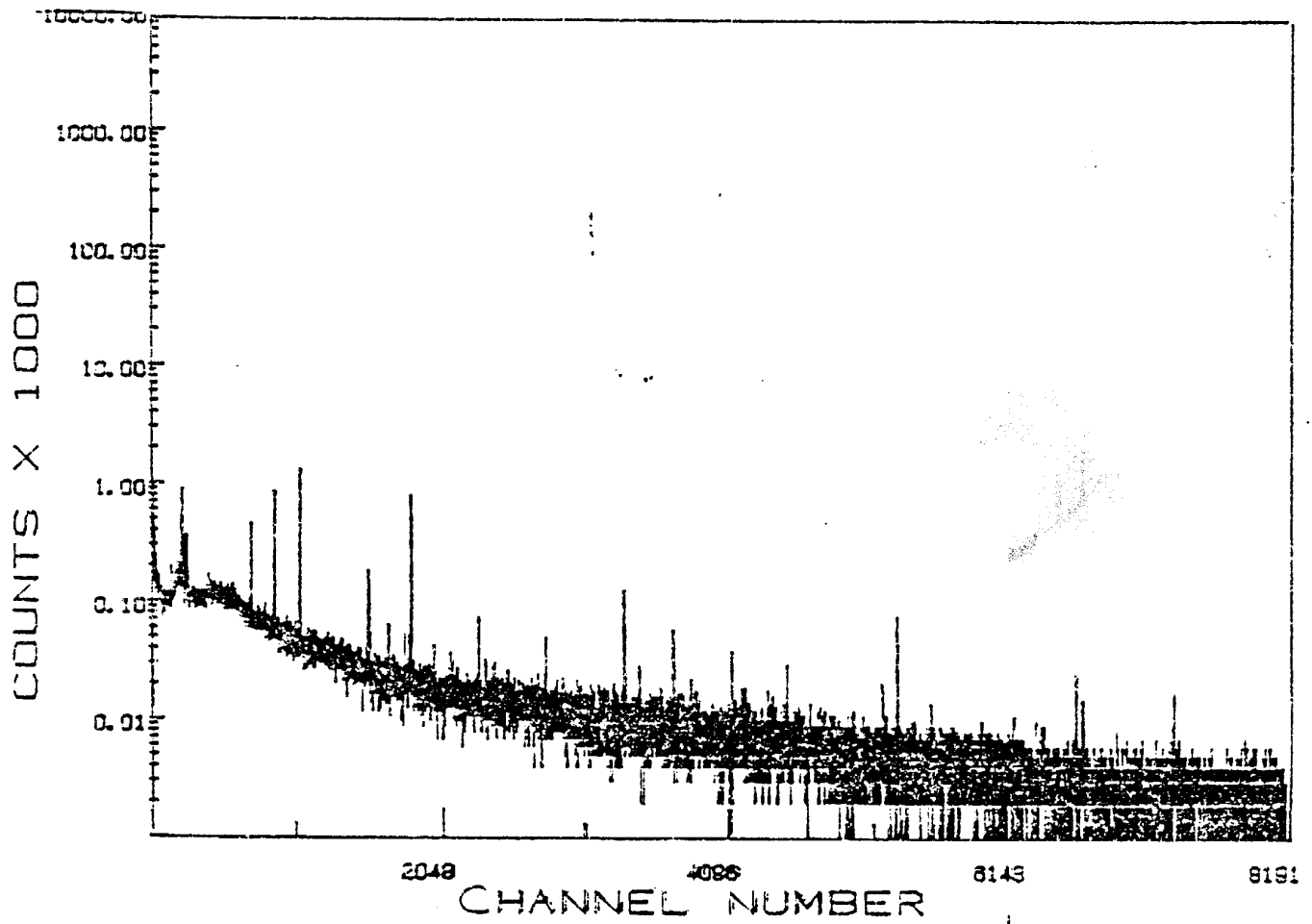


Figure 3

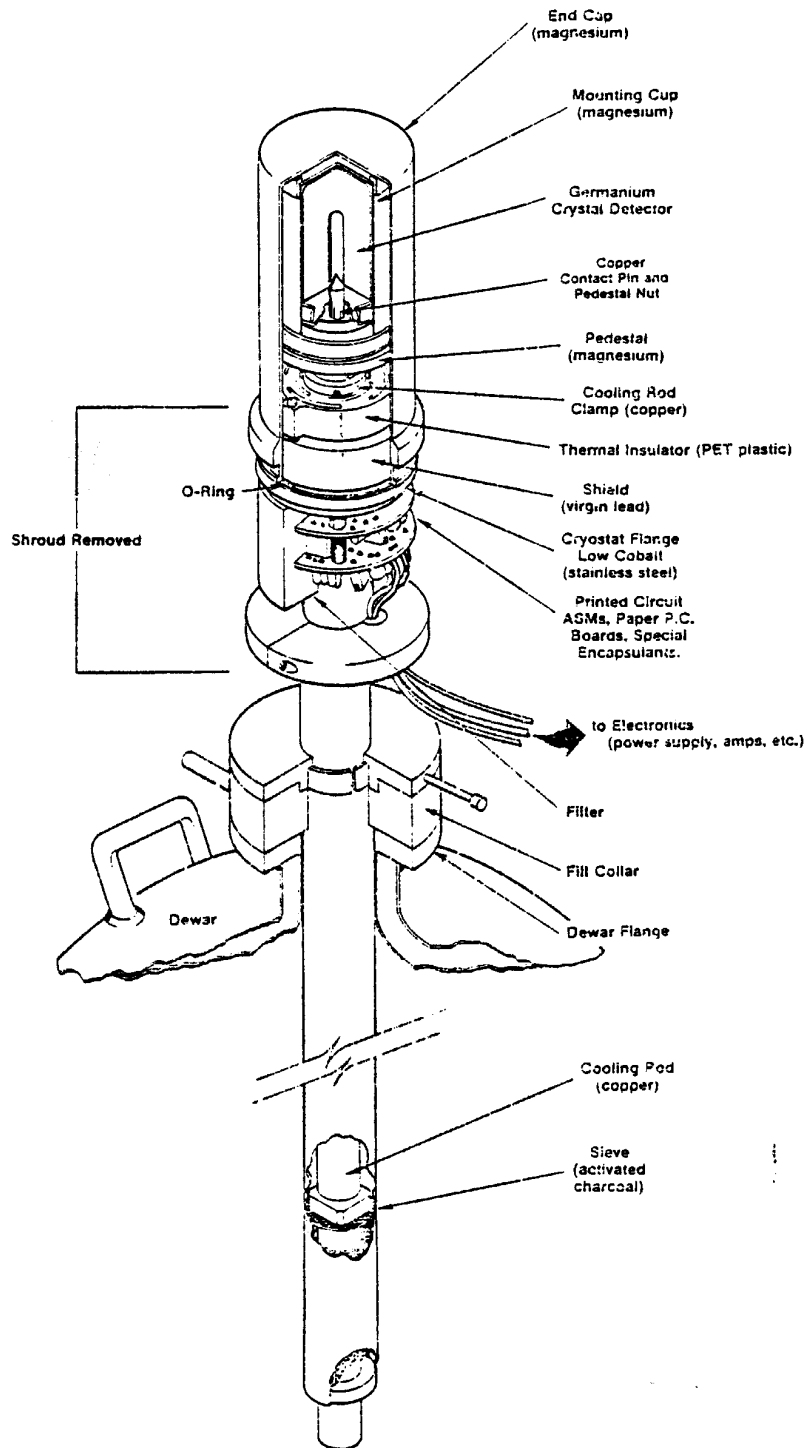


Figure 4

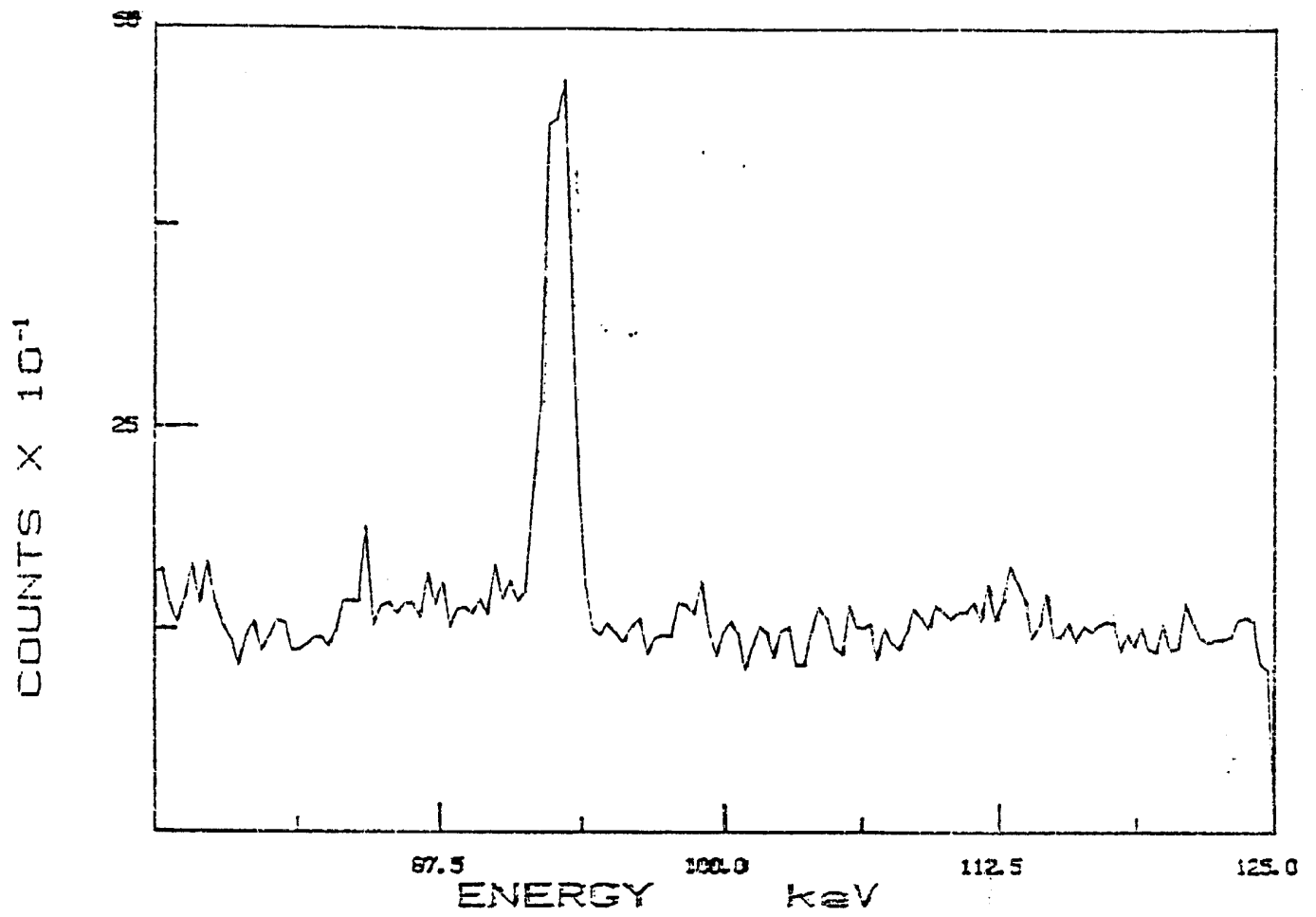


Figure 5

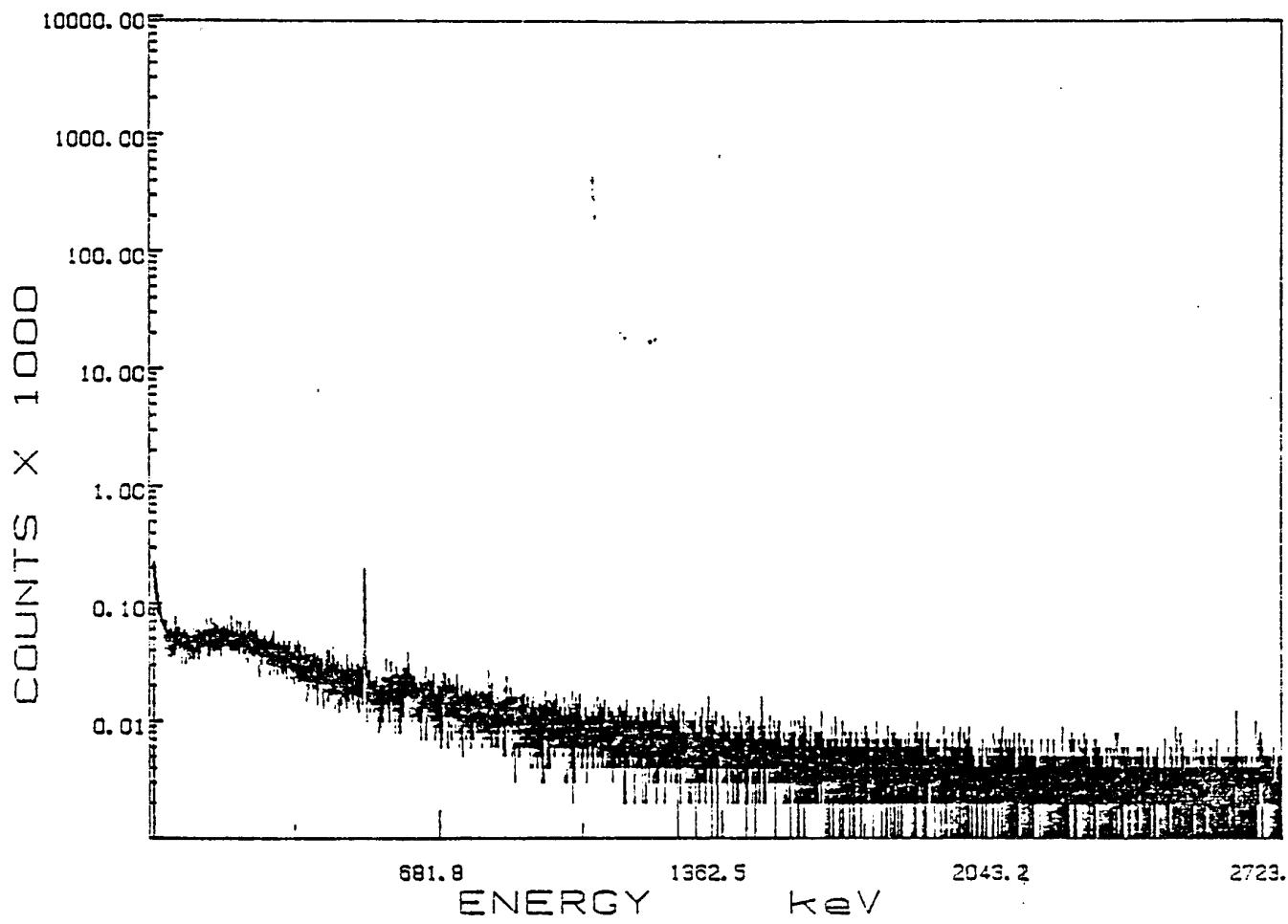


Figure 6

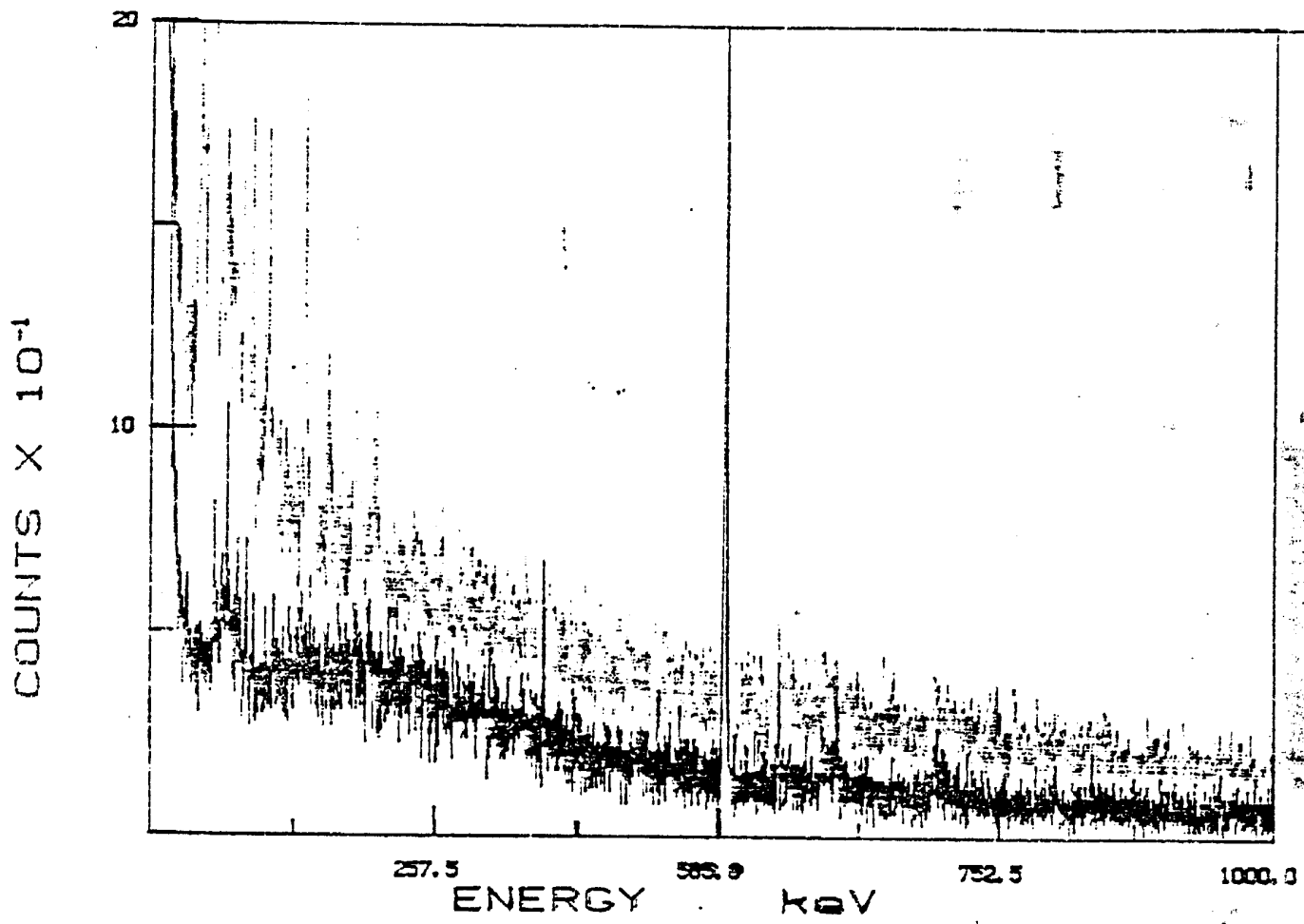


Figure 7

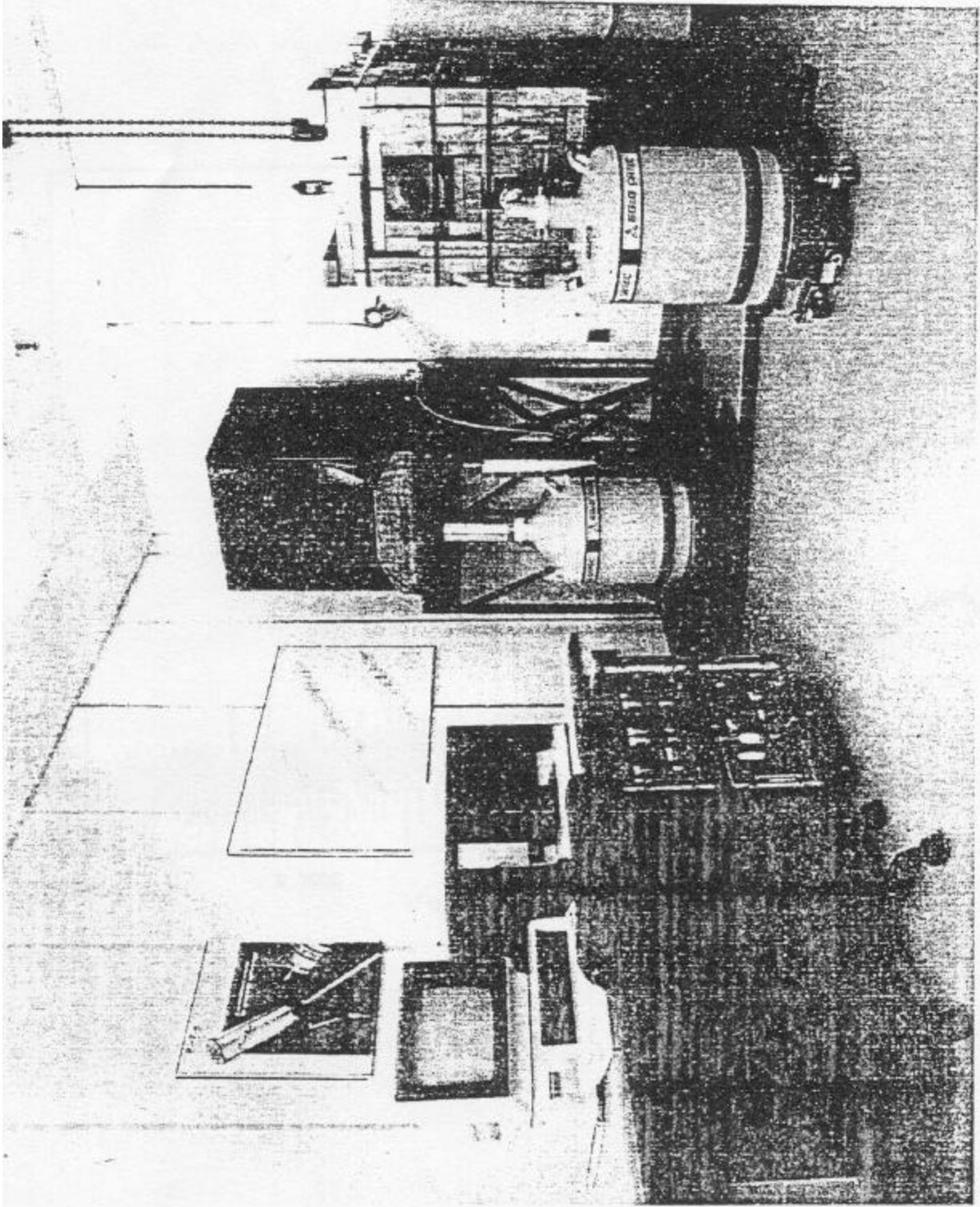


Figure 8

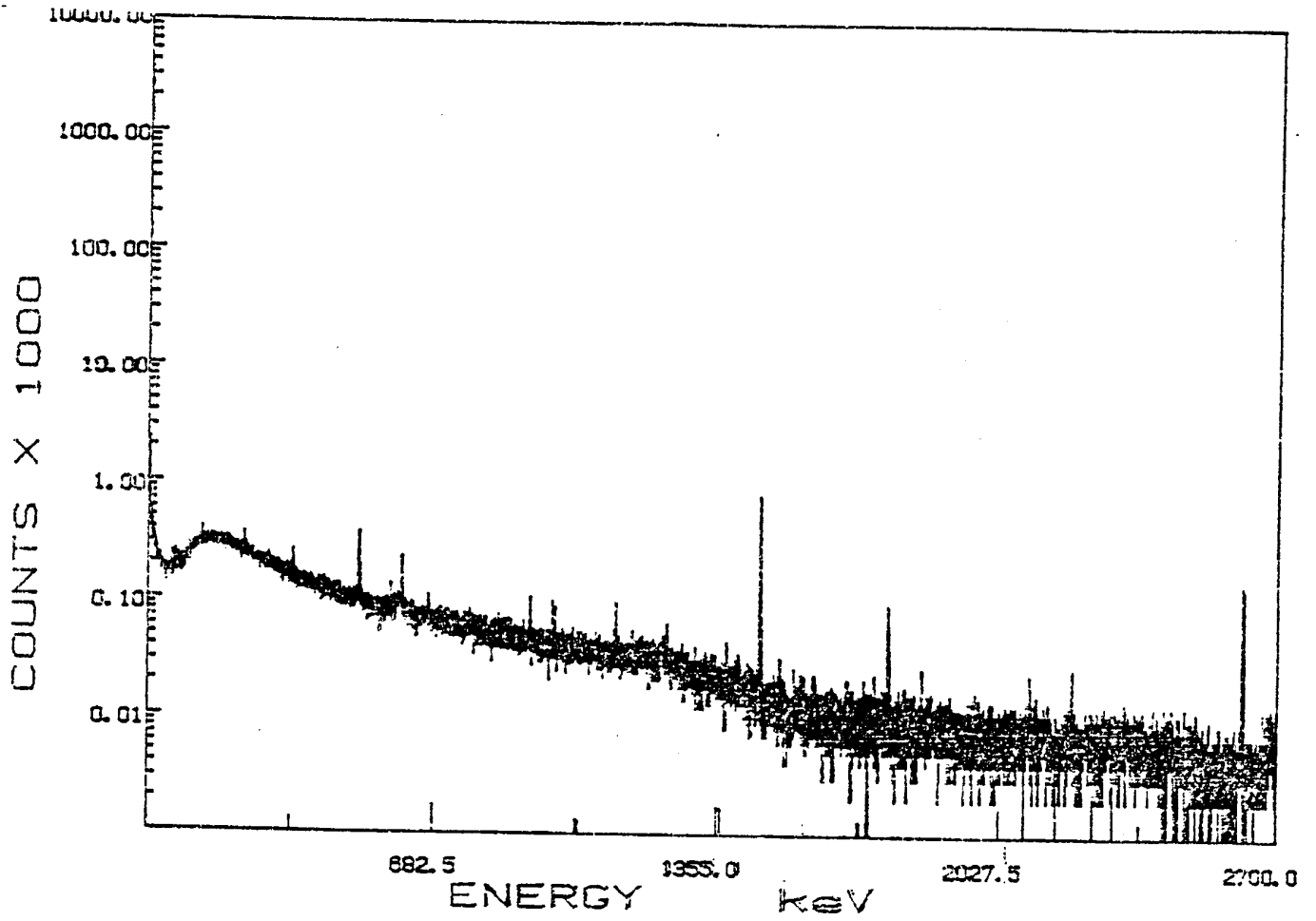


Figure 9

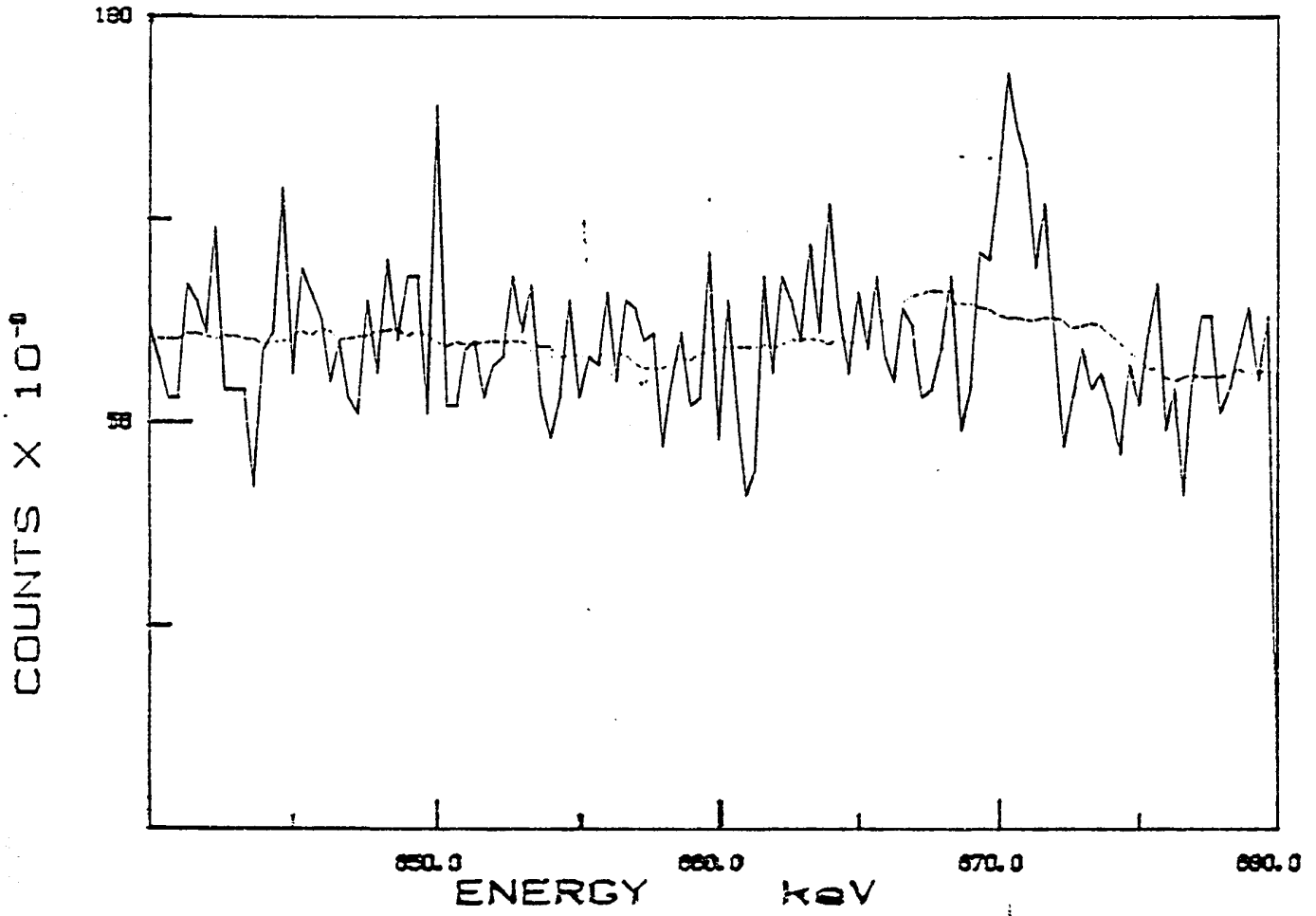


Figure 10

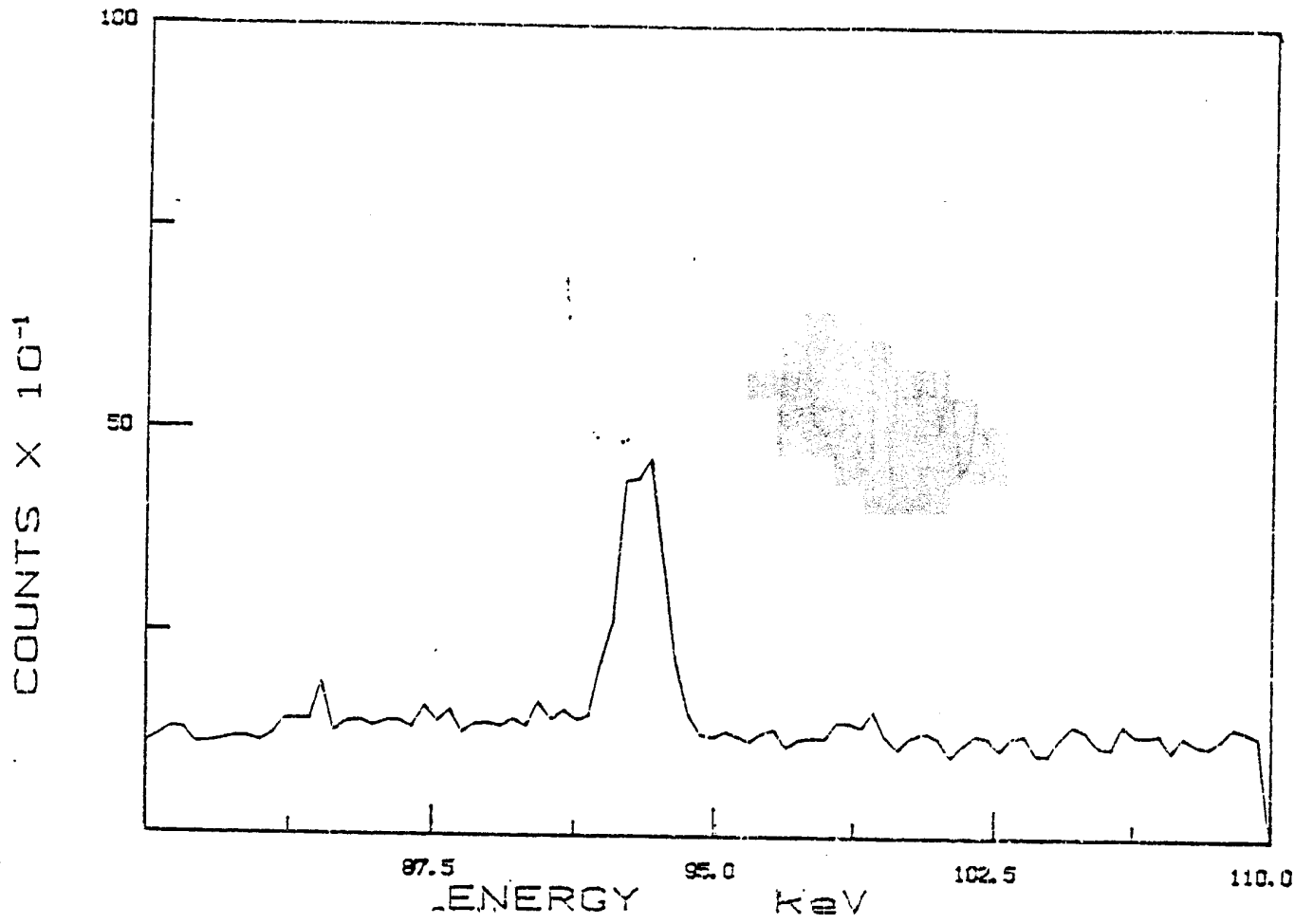


Figure 11

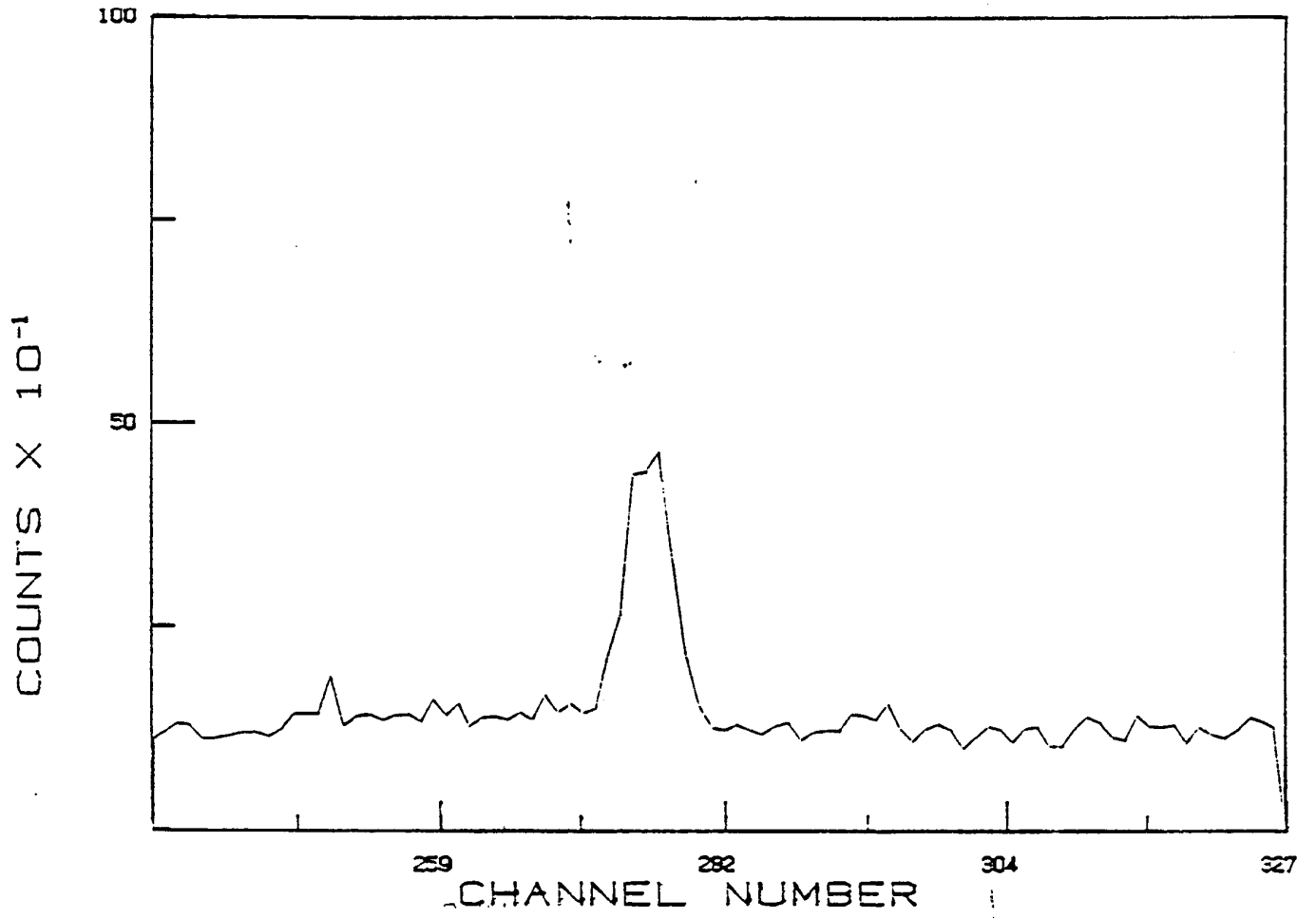


Figure 12

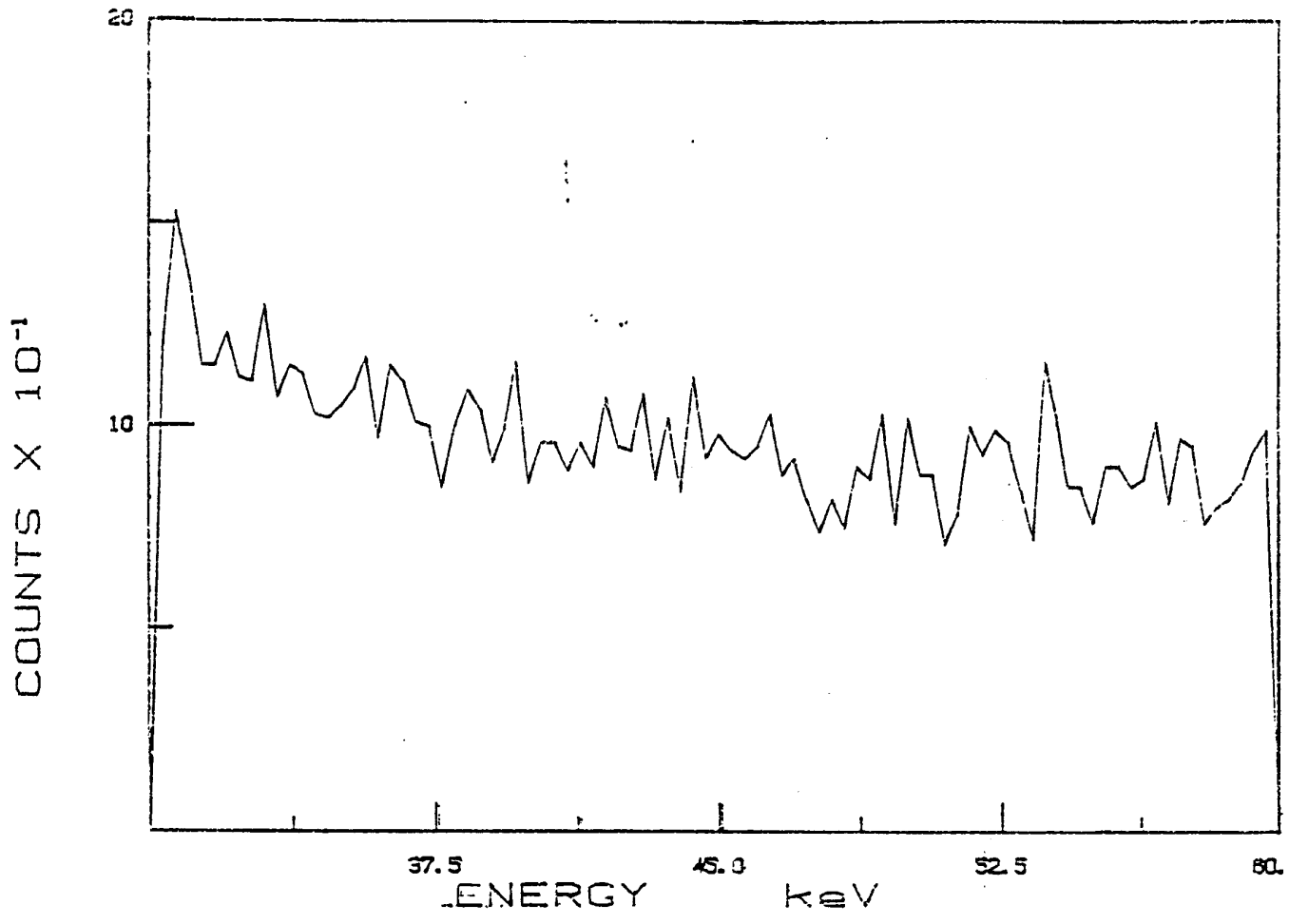
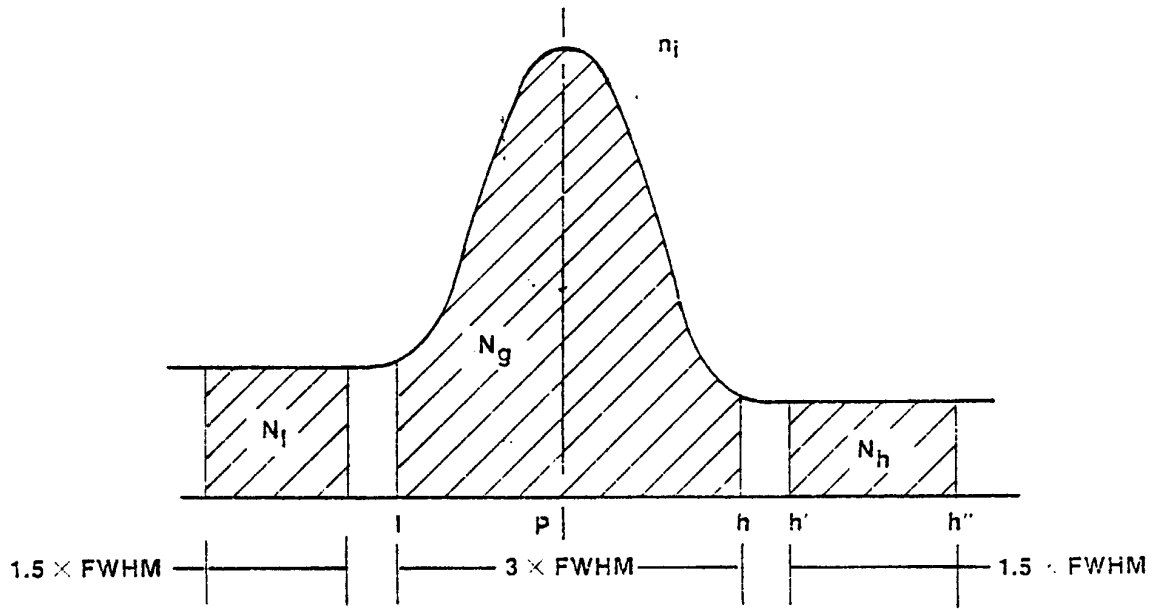


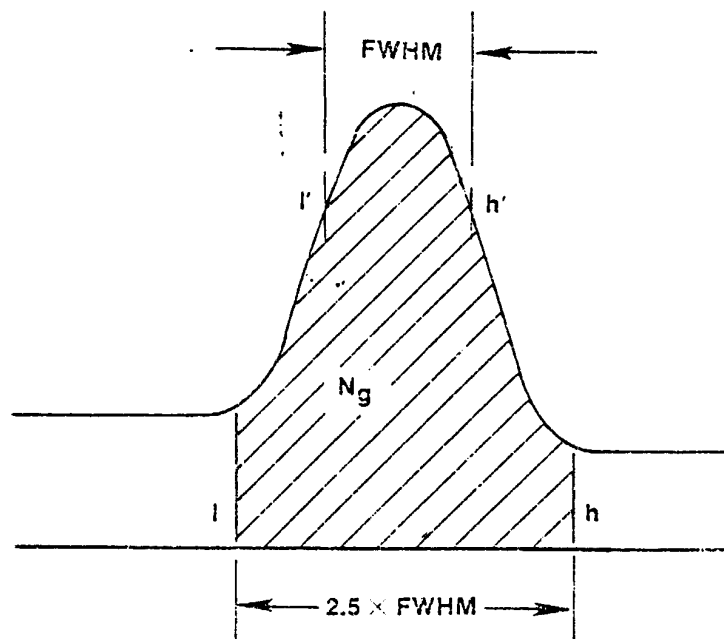
Figure 13



$$N_p = N_g - N_l - N_h$$

$$N_D = 2 \times \left[ 1 + \sqrt{1 + 2 \times (N_l + N_h)} \right]$$

Figure 14



$$N_D = \frac{N_g (h' - l' + 1)}{(h - l + 1)}$$

Figure 15

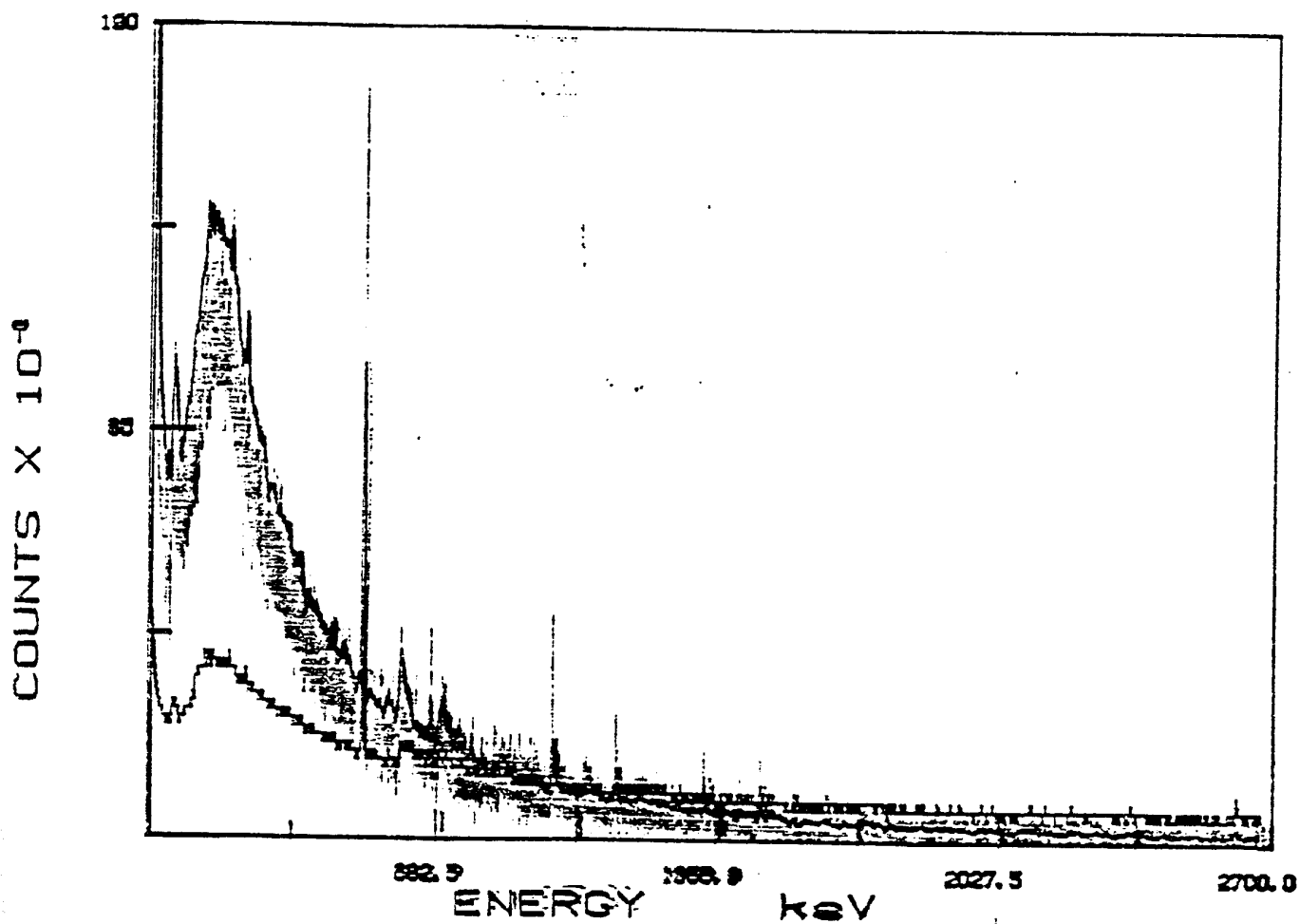


Figure 16

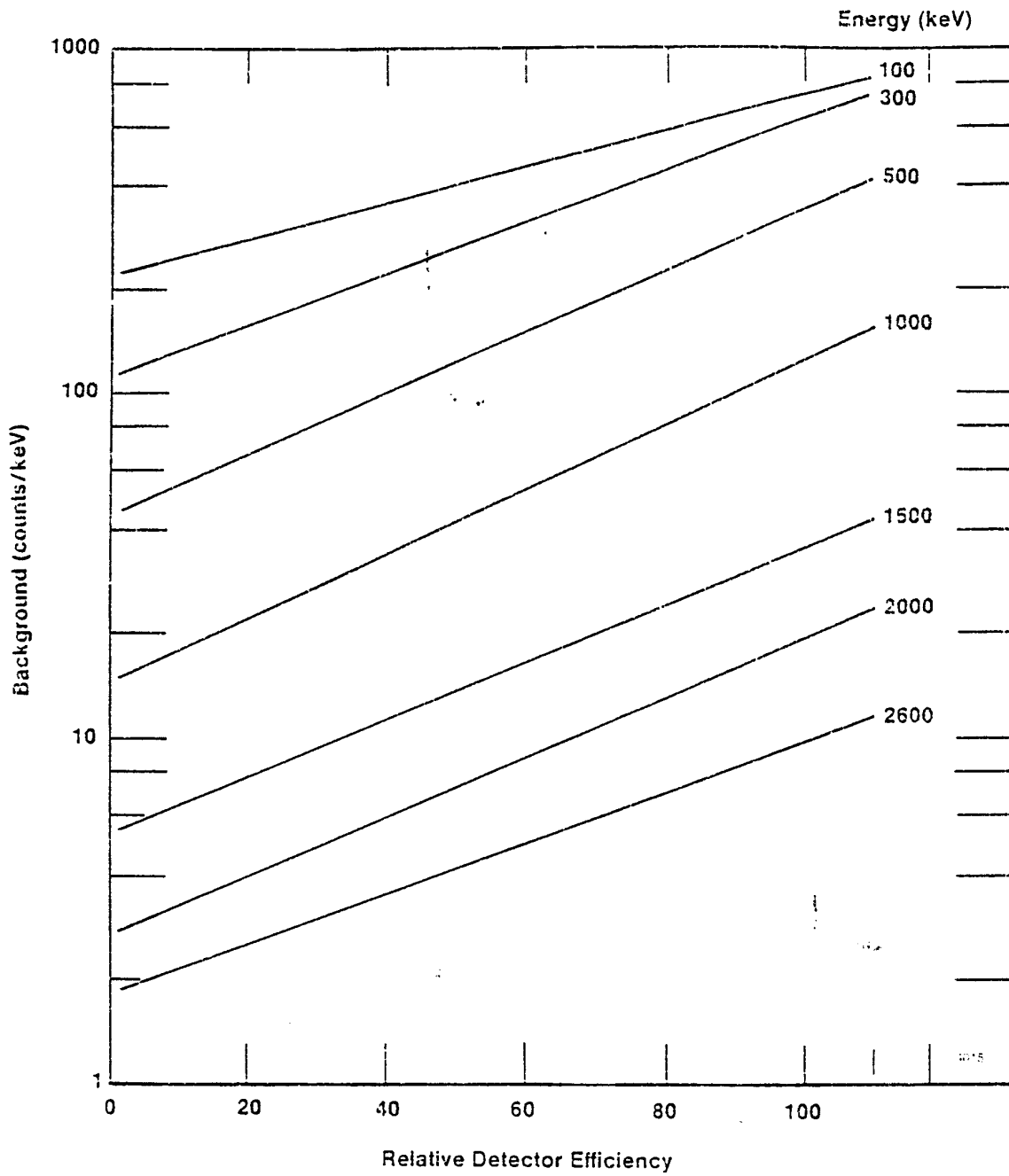


Figure 17

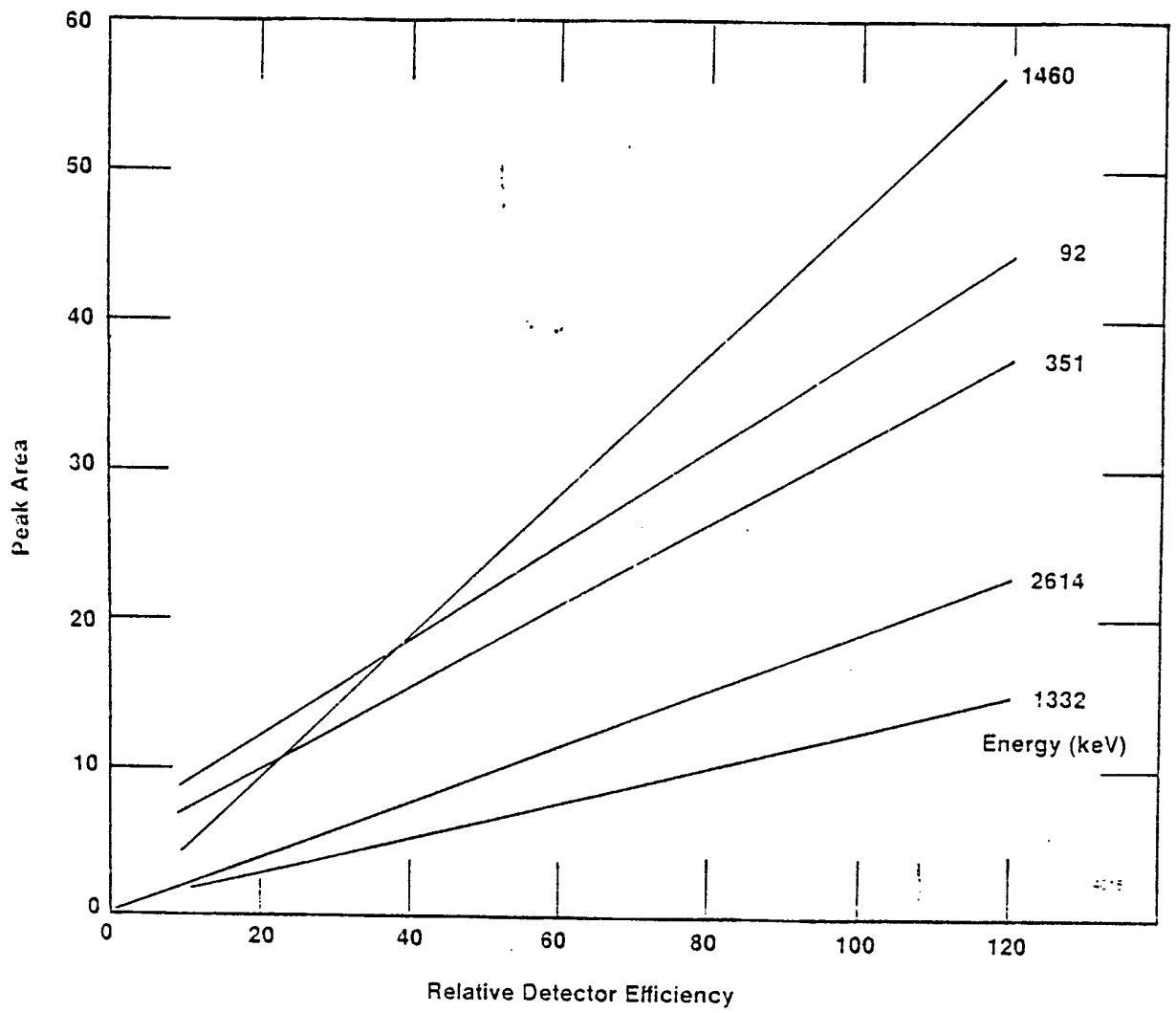


Figure 18